Phenomenology of electroweak bubbles and gravitational waves in the Littlest Higgs Model with T parity

Sahazada Aziz* and Buddhadeb Ghosh†

Center for Advanced Study, Department of Physics,

University of Burdwan, Burdwan-713104, India.

arXiv:1304.2997v2 [hep-ph] 12 Jan 2014

Abstract

We study the dynamics of electroweak bubbles in the scenario of a strong first order inverse electroweak phase transition at the TeV scale involving the global structure of the nonlinear sigma field in the littlest Higgs model with T parity. Employing the one-loop order finite temperature effective potential, we find that the pressure in the symmetric phase i.e., inside the bubble is always greater than that in the asymmetric phase i.e., outside the bubble, so that the bubbles are expanding. By calculating the fluid velocities in the two phases we arrive at the condition of a supersonic deflagrated motion of the bubble walls. We then discuss the generation of gravitational waves from the collisions of such bubbles as well as from the turbulence of the plasma.

PACS numbers: 98.80.Cq, 12.15.Ji, 04.30.-W.

Keywords: Early Universe; Electroweak phase transition; Beyond Standard Model.

* aziz_bu@rediff.com

† ghoshphysics@yahoo.co.in

I. INTRODUCTION

In recent years, dynamics of electroweak bubbles, associated with a first order phase transition, has been studied in the Standard Model (SM) [1-11] and its extensions [12-15], Two-Higgs Doublet Model (TDHM) [16], the Minimally Supersymmetric Standard Model (MSSM) [17, 18] as well as in model-independent way [19,20]. Also, aspects of gravitational waves (GW), as would be generated by bubble collisions and due to turbulence in the plasma have been investigated [21-28].

Knowledge of bubble dynamics and the concomitant CP violation [29] help us to understand the electroweak phase transition (EWPT) and electroweak baryogenesis (EWBG) scenario in more detail in a specific model.

Depending on the strength of the first-order phase transition and the nature of the finite-temperature effective potential (FTEP) in a model calculation, the motion of the bubble wall may belong to various categories, viz., deflagrations, detonations, hybrids or runaway [20]. Also, the motion can be supersonic, Jouguet or subsonic depending on whether the velocity of the plasma inside the bubble is greater than, equal to or less than the sound velocity in the medium, respectively. Usually, deflagrations are subsonic and detonations are supersonic. However, no clear-cut classification can be made in this regard. Although hydrodynamical equations give general features of bubble wall motion, microscopic analysis including friction of the bubble wall is necessary for getting the detailed information regarding the bubble wall velocity [13, 20].

Gravitational waves, which are considered to be the essential features of Einstein's General Theory of Relativity, have not been experimentally detected so far, although efforts are on in this direction [28]. Gravitational waves at the electroweak scale are believed to have been generated either by bubble wall collisions or by turbulence of the plasma.

The littlest Higgs model (L^2HM) [30] and the littlest Higgs model with T parity (LHT)[31-33] are economical beyond Standard Models (BSM) which can solve the little hierarchy problem. The LHT conforms to the electroweak precision data. In order to explore the prospects of EWPT and EWBG, finite-temperature calculations have been performed [34-36] in these models. In Ref. 36, an inverse strong first order EWPT has been observed in the global structure of the effective potential at the value of the physical Higgs field, $h = 1.1$ TeV with transition temperature, $T_c = 0.9$ TeV.

In Ref. 37, a two-step baryogenesis scenario associated with the inverse phase transition in the TeV scale has been presented. In the first step, the Universe makes a transition from an electroweak broken phase above T_c to a symmetric phase below T_c. Bubbles of symmetric phase are formed in the background of asymmetric phase. Baryon number violations take place within these bubbles due to sphaleron transitions induced by T even massless gauge boson fields. In the second step, a cross-over takes place at $T \approx 0.1$ TeV and the process of baryogenesis gets completed between the temperatures, 0.9 TeV and 0.1 TeV.

In view of the proposed new aspects [36] of the EWPT at the TeV scale and the associated EWBG scenario [37], we expect to find new features of the bubble dynamics as well as GW in the LHT.

The purpose of this paper is to examine the properties of the symmetric phase bubbles associated with an inverse strong first order EWPT and a new baryogenesis scenario therewith. In section II, we demonstrate the expansion of the symmetric phase bubbles. In section III, we calculate the bubble nucleation rate and time and in section IV, we study the bubble wall velocity. In section V we investigate the features of gravitational wave generation in our model. Finally, in section VI we make some concluding remarks.

II. EXPANSION OF THE SYMMETRIC PHASE BUBBLES

The presence of bubbles in the model under consideration is schematically shown in Fig.1. Here we have a situation which is opposite to that in the case of SM, viz., we have the symmetric phase bubbles in the background of the asymmetric phase. Whether these bubbles will contract or expand will depend on the difference of pressure in the two phases. The pressures are completely determined by the FTEP [36] and can be written as [4],

$$p_{in} = -V_{eff}\left(h = 0, T\right), p_{out} = -V_{eff}\left(h = 1.1\, TeV, T\right), \tag{1}$$

where, p_{in} and p_{out} are the pressures inside and outside the bubbles respectively. It should be noted that $h = 1.1\, TeV$ is the value of the physical Higgs field, where the phase transition is observed.

So far as the FTEP is concerned, two comments are in order here. Firstly, in the calculation of FTEP in Ref. 36, the effects of mirror fermions, which are instrumental in the non-minimal CP violation [38] in the LHT models, were not taken. Subsequently, we have

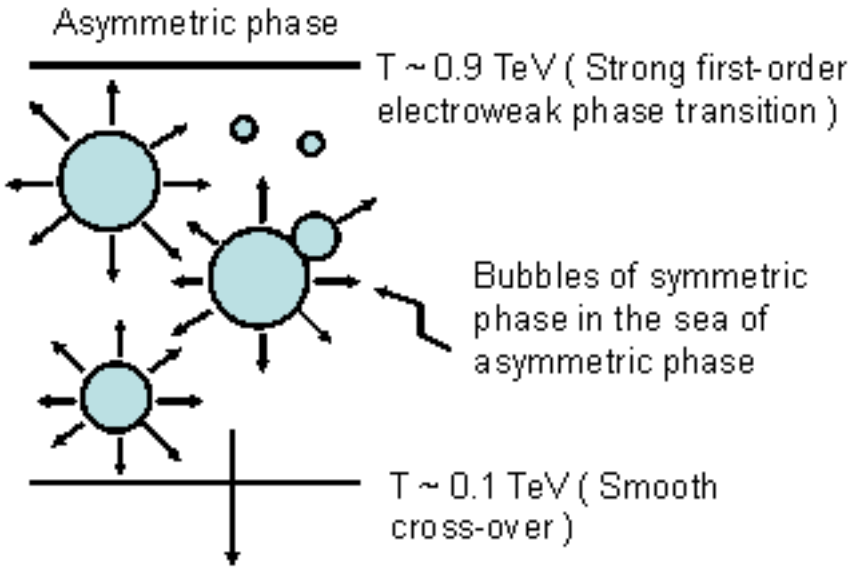


FIG. 1. Electroweak bubbles in the inverse phase transition scenario in the littlest Higgs model with T parity. Inside the bubbles, the VEV of the physical Higgs field, $< h >= 0$. Outside the bubbles, $< h >= 1.1$ TeV.

found that the inclusion of these fermions in the FTEP does not change the features of the phase transition - the value of T_c changes from 0.925 TeV to 0.905 TeV and the position of the minimum of the Higgs field remains the same. However, to be accurate, for the pressure calculations here, we have included the mirror fermions in the FTEP. The value of the mirror fermion coupling constant κ has been taken to be 0.7 consistent with a reasonable value of the mirror fermion mass, viz., 0.5 TeV [39]. The second comment concerns the recently discovered [40, 41] SM Higgs of mass, $m_H \simeq 125$ GeV at the LHC. This translates into value of Higgs quartic coupling constant, $\lambda = \frac{(m_H/v)^2}{2} \cong 0.13$, v being the SM Higgs VEV, 246 GeV. With this value of λ, we get a set of UltraViolet (UV) completion factors as $a = -0.01$, $a' = -0.0002$ for our FTEP, consistent with the experimental value of the SM Higgs VEV at zero temperature. Here the UV completion factors are defined as the quantities which take care of the physics above the cut-off scale, $\Lambda \approx 4\pi f \approx 10\, TeV$, where f is the high energy symmetry breaking scale. It may be noted here that the general procedure for obtaining the UV completion factors in our model is described in Ref. 36.

With the above considerations and Eq.1 we have calculated the quantity, $(p_{in} - p_{out})$ of

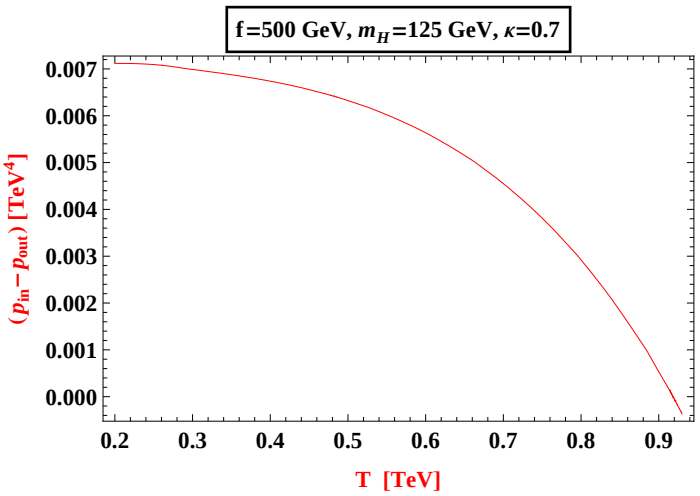


FIG. 2. Excess pressure within the bubbles of the symmetric phase as a function of temperature.

which the plot is shown in Fig.2. We observe that the excess pressure within the symmetric phase bubbles is always positive. From this we may conclude that after the inverse EWPT at T_c=0.9 TeV, the symmetric phase bubbles will expand in the background of the asymmetric phase.

III. NUCLEATION RATE AND TEMPERATURE

The excess free energy [3] in a true vacuum bubble, which is a symmetric phase bubble in the present case, can be written as,

$$\Delta F(T) = 4\pi \int_0^R r^2 \left[\frac{1}{2} \left(\frac{dh}{dr} \right)^2 + V(h,T) \right] dr, \tag{2}$$

where, we have assumed that the bubble is spherical and R is the radius of the bubble. $\Delta F(T)$ is the same as the three-dimensional Euclidean action, S_3 [42] which is related to the four-dimensional Euclidean action S_E as $S_3 = S_E/T$ in the imaginary time formalism of finite-temperature field theory. Eq.2 is the energy which causes the symmetric phase bubble to expand in the present scenario. The derivative term in Eq.2 corresponds to a surface energy and the potential term a volume energy. In the thin wall approximation, appropriate for a strong first-order phase transition, the derivative of the Higgs field can be written as [42], $\pm\sqrt{2V\,(h,T)}$ in the limit of exact degeneracy of the potential minima at $T = T_c$. A positive value of the derivative would reflect the fact that in our case as we go from the centre of a symmetric phase bubble to the boundary, the VEV of h increases

from 0 to 1.1 TeV. To avoid using an ansatz of the field in the r space, we then change the integration variable from r to h and approximate the surface term as, $4\pi R^2\sigma(T)$, where $\sigma(T) = \int_{h=0}^{h=1.1}\sqrt{2V\,(h,T)}dh$ can be called the surface energy density. We also write the volume term in Eq.2 as $\frac{4}{3}\pi R^3\bar{V}(h,T)$ where $\bar{V}(h,T)$ is an average effective potential inside the bubble. Since the potential inside the bubble should be measured with respect to that outside, we can write $\bar{V}(h,T) = V_{in} - V_{out} = -p_{in} - (-p_{out}) = -(p_{in} - p_{out}) = -\Delta p$. Thus, we write the volume term as, $-\frac{4}{3}\pi R^3\Delta p(T)$.

Now, we get the radius of a critical bubble by minimizing $\Delta F\,(T)$ from the equation, $\left[\frac{\delta\Delta F(T)}{\delta R}\right]_{R=R_c} = 0$ with $\Delta F(T) = 4\pi R^2\sigma(T) - \frac{4}{3}\pi R^3\Delta p(T)$ and thus $R_c(T) = \frac{2\sigma(T)}{\Delta p(T)}$.

The bubble nucleation rate per unit time per unit volume can be written in terms of the excess free energy $\Delta F_C(T)$ of the critical bubble as [43,18],

$$\Gamma_N\,(T) \simeq T^4\left[\frac{\Delta F_C(T)}{2\pi T}\right]^{3/2} exp\left[-\frac{\Delta F_C(T)}{T}\right] \tag{3}$$

The bubble nucleation temperature T_N, which is somewhat lower than T_c in the case of first order phase transition, is defined as the temperature at which the rate of nucleation of a critical bubble within a horizon volume is equal to the Hubble parameter at that temperature. Since the horizon scale is approximately $H(T)^{-1}$ the nucleation temperature can be defined by the equation,

$$\frac{\Gamma_N(T_N)}{H^3(T_N)} \simeq H(T_N) \simeq 1.66\sqrt{g_*(T_N)}\frac{T_N^2}{m_{Pl}} \tag{4}$$

where $g_*(T)$ is the relativistic degrees of freedom and $m_{Pl} \simeq (1.22\times 10^{16} TeV)$ is the Planck mass. From Eqs. (3) and (4), we get,

$$\frac{\Delta F_C(T_N)}{T_N} - \frac{3}{2}\ln\left[\frac{\Delta F_C(T_N)}{T_N}\right] - 143.46 + 2\ln\left[g_*(T_N)\right] + 4\ln T_N \simeq 0 \tag{5}$$

Eq.5 can be graphically solved for T_N. Denoting the LHS of Eq.5 as $f(T_N)$, we show in Fig.3 a plot of $f(T_N)$ vs. T_N. The graph shows that $f(T_N) \simeq 0$ for $T_N \sim 0.5 - 0.6$ TeV. The nucleation temperature can also be determined from the consideration of the fact that the space-time integrated nucleation rate (i.e., the nucleation probability) should be of order 1[13]:

$$\int_{t_C}^{t_N}\Gamma_N(t)V_C dt \sim 1 \tag{6}$$

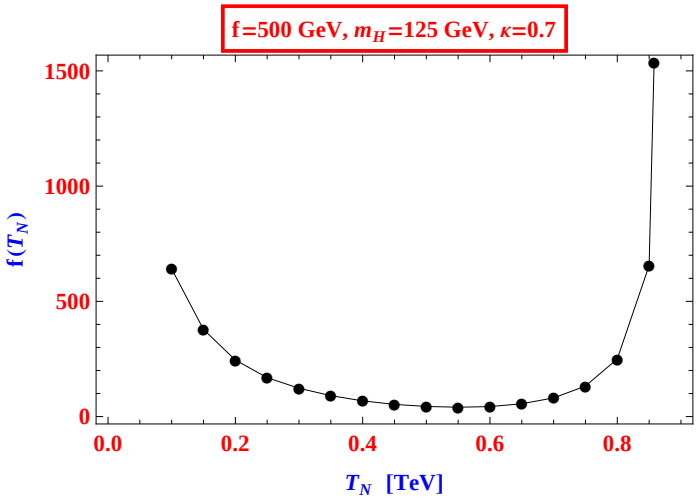


FIG. 3. A plot of $f(T_N)$ vs. T_N where $f(T_N)$ is the function on the left hand side of Eq.5 and T_N is the bubble nucleation temperature.

Now the horizon scale is roughly $2t$ and so, volume $= (2t)^3$. Using the time-temperature relations [42, 13],

$$t = 0.301 g_*^{-1/2} \frac{m_{Pl}}{T^2},$$
$$\frac{dT}{dt} = -HT \tag{7}$$

we get the integral in Eq.6, which is the total nucleation probability of a single bubble, as,

$$I = \left(0.602 g_*^{-1/2} m_{Pl}\right)^4 (2\pi)^{-3/2} \int_{T_N}^{T_c} T^{-13/2} [\Delta F_C(T)]^{3/2} exp\left[-\Delta F_C(T)/T\right] dT \tag{8}$$

Results of evaluation of this integral for different values of T_N are shown in Table 1. We see from Table 1 that consistent with Eq.6, the value of T_N should be 0.635 TeV.

IV. THE NATURE OF BUBBLE AND WALL VELOCITY

The entropy, energy and enthalpy densities are defined in terms of the pressure $p(T)$ as,

$$s(T) = (dp(T))/dT \equiv p'(T),$$
$$\rho(T) = Ts(T) - p(T),$$
$$\omega\left(T\right) = \rho\left(T\right) + p\left(T\right) = TS(T). \tag{9}$$

TABLE I. Nucleation temperature, excess free-energy and the nucleation probability (integral I in Eq.8).

T_N(TeV)	$\Delta F_C(T_N)$	value of integral (I)
0.55	100.91	1.37×10^{10}
0.60	111.53	1.07×10^{5}
0.61	114.43	4.35×10^{3}
0.62	117.72	113.87
0.63	120.94	3.22
0.635	122.76	0.429
0.64	124.56	0.058
0.65	128.63	6.45×10^{-4}
0.66	133.04	4.88×10^{-6}
0.67	137.98	2.05×10^{-8}
0.70	156.32	3.07×10^{-17}

We have then the following equations, valid for a first-order phase transition.

$$\begin{aligned} p_+(T_c) &= p_-(T_c), \\ s_+(T_c) &\neq s_-(T_c), \\ \rho_+(T_c) &\neq \rho_-(T_c), \\ \text{and } \omega_+(\mathrm{T_c}) &\neq \omega_-(\mathrm{T_c}), \end{aligned} \tag{10}$$

where, the quantities with the subscript, '+' refer to those in the high-temperature phase (i.e., the phase outside the bubble) and the subscript, '−' is for the quantities in the low-temperature phase (i.e., the phase inside the bubble).

The latent heat L is defined as the difference between the energy densities of the two phases at $T = T_c$ and thus,

$$L = T_c[p'_+(T_c) - p'_-(T_c)] \tag{11}$$

Solving hydrodynamical equations [20,44,45], we get,

$$\omega_+\gamma_+^2 v_+ = \omega_-\gamma_-^2 v_-,$$
$$\omega_+\gamma_+^2 v_+^2 + p_+ = \omega_-\gamma_-^2 v_-^2 + p_- \tag{12}$$

where, $\gamma = 1/\sqrt{1-v^2}$, v being the velocity being assumed to be aligned in a particular direction, say, the z-direction.

Equivalently, we get,

$$v_+ v_- = \frac{p_+ - p_-}{\rho_+ - \rho_-},\ \frac{v_+}{v_-} = \frac{\rho_- + p_+}{\rho_+ - p_-} \tag{13}$$

whence, we obtain,

$$v_+ = \sqrt{\frac{(p_+ - p_-)(\rho_- + p_+)}{(\rho_+ - \rho_-)(\rho_+ - p_-)}},$$
$$v_- = \sqrt{\frac{(p_+ - p_-)(\rho_+ - p_-)}{(\rho_+ - \rho_-)(\rho_- + p_+)}} \tag{14}$$

where, it is implied that, $p_+ = p_+(T_+)$, $p_- = p_-(T_-)$ etc., T_+ being the temperature outside the bubble and T_- inside.

The bubble motions can be broadly classified as [13],

(i) Deflagration : The velocity of the plasma inside the bubble is more than outside, $v_- > v_+$,

(ii) Detonation : The velocity outside is more than inside, $v_+ > v_-$.

Deflagration may further be subdivided as, strong: $v_- > c_s$, Jouguet: $v_- = c_s$ and weak: $v_- < c_s$. Here, c_s is the velocity of sound inside the bubble, which has the value $1/\sqrt{3}$ for a relativistic plasma [13]. The strong deflagration is therefore supersonic and the weak deflagration is subsonic. A detonation will be called strong if $v_- < c_s$, Jouguet if $v_- = c_s$ and weak if $v_- > c_s$.

Deflagrations and detonations are also characterized by the following temperature constraints [13, 19, 20]:

$$\mathrm{Deflagration : T_+ > T_N > T_-},$$
$$\mathrm{Detonation : T_- > T_+ = T_N}. \tag{15}$$

The above characterizations show that the detonation cases are easier to investigate because of the condition, $T_+ = T_N$.

Now, coming to the case of LHT, let us first assume that the bubble motion is detonated, so that $T_+ = T_N$=0.635 TeV. Fig.4 shows the result of calculation of v_+ and v_- as a function of T_- for the parameter space $f = 500$ GeV, m_H =125 GeV, $\kappa = 0.7$ and $T_+ = T_N$ (= 0.635 TeV). The plot clearly shows that $v_- > c_s > v_+$, which is in contradiction with the velocity characterization of detonation. Hence we can rule out the case of detonation in the case of LHT. Also as $v_- > c_s$ in Fig.4, we are getting an indication of *supersonic deflagration* [19] for the bubble wall motion here.

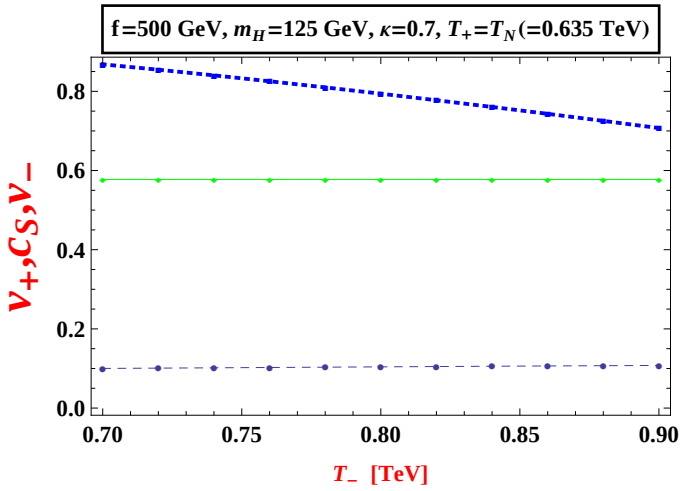


FIG. 4. Assumming detonation motion ($T_+ = T_N$), plot of velocity of plasma outside the bubble: v_+(lower plot: blue-dashed), sound velocity: $c_S(= \frac{1}{\sqrt{3}})$, middle green straight line) and velocity of plasma inside the bubble: v_-(upper plot: blue-dotted).

To study the bubble wall motion, let us use the following so-called bag equations of state [13]:

$$\rho_+ = a_+ T^4 + \varepsilon,\ p_+ = \frac{1}{3} a_+ T^4 - \varepsilon,\ \rho_- = a_- T^4,\ p_- = \frac{1}{3} a_- T^4 \tag{16}$$

and the entropy density,

$$s_\pm = \frac{4}{3} a_\pm T^3, \tag{17}$$

where,

$$a_\pm = \frac{\pi^2}{30} g_*(T_\pm) \tag{18}$$

are numbers related to the number of relativistic species present in the plasma. It is interesting to see the physical significance of the quantity ε. Since at T_c, the pressure difference

between the two phases is zero, we get from Eq.16,

$$(a_+ - a_-)\, T_c^4 = 3\varepsilon \tag{19}$$

Then, from the expressions of entropy and latent heat we get,

$$L = 4\varepsilon \tag{20}$$

which shows that ε is closely related to the amount of latent heat L of phase transition.

We now define two important quantities upon which the bubble wall velocity depends:

$$\alpha = \frac{\varepsilon}{a_+ T_+^4},\ \alpha_N = \frac{\varepsilon}{a_+ T_N^4}. \tag{21}$$

From hydrodynamics, we get a relationship between the plasma velocities in terms of α as [46],

$$v_+ = \frac{\frac{1}{6v_-} + \frac{v_-}{2} \pm \sqrt{\left(\frac{1}{6v_-} + \frac{v_-}{2}\right)^2 + \alpha^2 + \frac{2}{3}\alpha - \frac{1}{3}}}{1+\alpha} \tag{22}$$

where, the $+(-)$ sign corresponds to the detonated (deflagrated) motion of the bubble. As we have argued earlier, the motion of the bubble is deflagrated rather than detonated. Accordingly, we shall study, henceforth, the deflagrated motion of the bubble, taking the '$-$' sign in Eq.22.

A deflagrated bubble proceeds via the generation of shock waves. The expressions of the velocities v_1 and v_2 of the fluid before and behind respectively of the shock front in the frame of the shock front are [13],

$$|v_1| = \frac{1}{\sqrt{3}} \left(\frac{3T_+^4 + T_N^4}{3T_N^4 + T_+^4}\right),\ |v_2| = \frac{1}{3\,|v_1|} \tag{23}$$

In the laboratory frame the fluid within the bubble, i.e., behind the bubble wall is at rest, as the bubble is isotropically expanding, and also ahead of the shock front, where the temperature is T_N, which belongs neither to the low-temperature nor to the high temperature phase, the fluid is at rest. Thus, the wall velocity in the laboratory frame,

$$v_w = -v_-, v_{sh} = -v_1, \tag{24}$$

because, v_- is the velocity of the fluid inside the bubble in the reference frame of the wall. In Eq.24 v_{sh} denotes the velocity of the shockfront. Thus in terms of the bubble wall velocity also, it can be said that the motion is supersonic if we can show that $v_- > c_s$ for all

temperatures T_+ outside the bubble. The fluid velocity v_f between the two fronts can be written either in terms of v_1, v_2 or v_+, v_-:

$$v_f = \frac{v_2 - v_1}{1 - v_1 v_2} = \frac{v_+ - v_-}{1 - v_+ v_-} \tag{25}$$

Putting the values of v_1 and v_2 we get,

$$\frac{v_+ - v_-}{1 - v_+ v_-} = \frac{\sqrt{3}(\alpha - \alpha_N)}{\sqrt{3\,(\alpha_N + \alpha)\,(3\alpha + \alpha_N)}} \tag{26}$$

Eliminating v_+ from Eqs.25 and 26 we get an expression of v_- in terms of α and α_N:

$$\begin{aligned} v_- = {} & (\sqrt{3}(\alpha_+ - \alpha_N)(3\alpha_+ + \alpha_N)(\alpha_+ + 3\alpha_N))^{-1} \\ & \left(\begin{array}{l} \sqrt{(3\alpha_+ + \alpha_N)(\alpha_+ + 3\alpha_N)}(\alpha_+^2 - 2\alpha_+(1 + 4\alpha_+)\alpha_N + \alpha_N^2) \\ +2\sqrt{((3\alpha_+ + \alpha_N)(\alpha_+ + 3\alpha_N)(8\alpha_+^3\alpha_N^2 + \alpha_N^4 - 2\alpha_+^2\alpha_N^2(1 + 2\alpha_N) \\ +\alpha_+^4(1 + 4\alpha_N(-1 + 4\alpha_N))) \end{array} \right) \end{aligned} \tag{27}$$

In LHT, $g_*(T \geq 500\,GeV) \simeq 214$, T_N=0.635 TeV, T_c=0.91 TeV, L=0.2464 TeV. Then we get, $\alpha_N = 0.00538$..

Keeping the latent heat and therefore α_N constant, we calculate v_- varying α. A plot of v_- against α(Fig.5) shows that the motion of the fluid inside the bubble, and therefore the bubble wall velocity v_w in the laboratory frame is supersonic. We can also plot v_- against

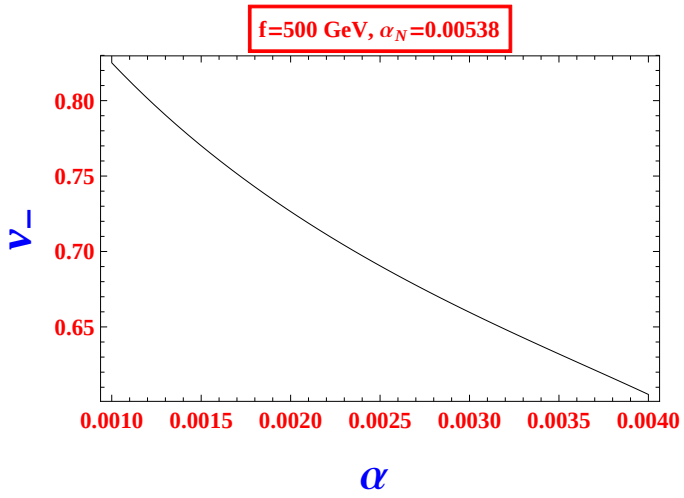


FIG. 5. Plot of v_- against α for fixed α_N following Eq.27. For various values of the temperature T_+, v_- is always greater than the sound velocity, c_s=$1/\sqrt{3}$=0.577.

α for various values of v_+ following Eq.22 instead of Eq.27 where v_+ has been eliminated. Such graphs are shown in Fig.6. It is seen from these graphs that for various values of v_+ also the supersonic nature of wall velocity i.e., $v_w = |v_-| > c_s$ is maintained.

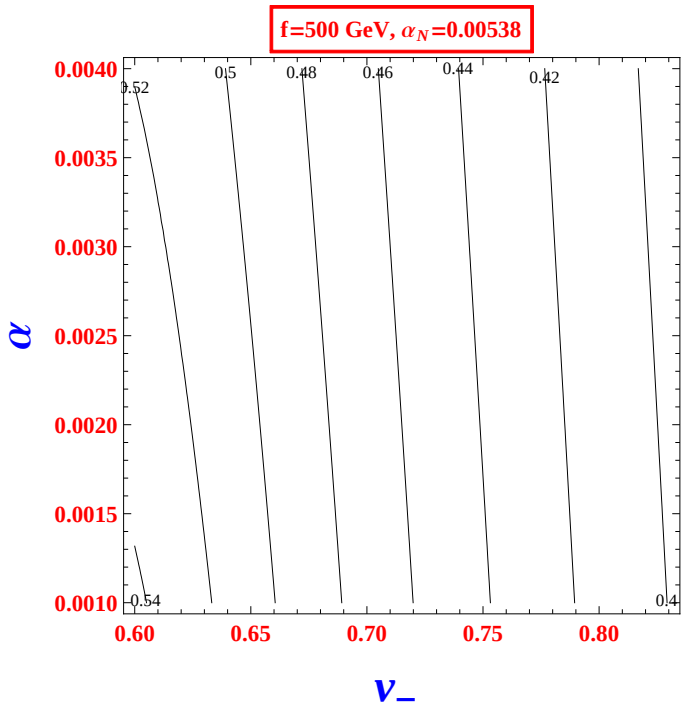


FIG. 6. Contour plot of v_- against α for various values of v_+. Contours denote the values of v_+.

V. GRAVITATIONAL WAVES

Gravitational waves [48-50] may be generated at the time of the first-order EWPT by two mechanisms [21-28]: (i) Collision of bubble walls, (ii) Turbulence created by the bubble expansion. Since the strong first-order phase transition is not possible in the SM, GW cannot be generated within the framework of the SM.

The frequency and energy density of GW produced in the early Universe change due to the expansion of the Universe. The frequency varies as a^{-1} and the energy density a^{-4} where a is the scale factor. Thus the red-shifted frequency we observe today is given by,

$$f_0 = f\frac{a}{a_0}, \tag{28}$$

where, a_0 is the scale factor at the present time and $a(f)$ is the scale-factor (frequency) at the early Universe, i.e. at the time of the origin of the GW.

Now, because of the adiabatic expansion of the Universe, we can write,

$$a^3 g_* T^3 = {a_0}^3 g_0 {T_0}^3 \tag{29}$$

Substituting, $T_0 = 2.73K = 2.35 \times 10^{-13}\,GeV$ and $g_0 = 2$ we get,

$$\frac{a}{a_0} = 6.4 \times 10^{-16}\left(\frac{100}{g_*}\right)^{1/3}\left(\frac{100\,GeV}{T}\right). \tag{30}$$

The wavelength of GW in the early Universe should be a fraction of the Hubble size H^{-1}. Hence, it is instructive to write f_0 in terms of f/H. Thus, we write,

$$f_0 = \left(\frac{a}{a_0}\right)\left(\frac{f}{H}\right)H, \tag{31}$$

where, H is given by the Friedmann equation,

$$H^2 = \frac{8\pi G}{3}\rho, \tag{32}$$

ρ being the radiation energy density,

$$\rho = \frac{\pi^2 g_* T^4}{30}. \tag{33}$$

From the above equations, we get a suggestive expression of frequency of GW in the present Universe,

$$f_0 = 1.32 \times 10^{-5}\Big(\frac{g_*}{100}\Big)^{1/6}\left(\frac{f}{H}\right)\left(\frac{T}{100\,GeV}\right)\text{Hz}, \tag{34}$$

where, we have used the numerical values [42], $m_{Pl} = 1.22 \times 10^{19}\,GeV$ and $1\,GeV^{-1} = 6.5822 \times 10^{-25}\,\text{sec}^{-1}$.

Let us first consider GW generation from bubble wall collisions. During EWPT, the bubble nucleation rate per unit time and unit volume may be written as [28, 51],

$$\Gamma_{\rm N}\,(t) = \Gamma_0\,(t_i)\,e^{\beta(t-t_i)}, \tag{35}$$

where, t_i is an initial time and β is a parameter setting the time and length scales of the phase transition as β^{-1} and $v_w\beta^{-1}$ respectively, v_w being the bubble wall velocity. Assuming $f \sim \beta$, we can write from Eq.34,

$$f_0^{coll} = 1.32 \times 10^{-5}\Big(\frac{g_*}{100}\Big)^{1/6}\left(\frac{T}{100\,GeV}\right)\left(\frac{\beta}{H}\right)\text{Hz}. \tag{36}$$

A recent simulation [21, 28] gives the dependence of the peak frequency, f_{peak}^{coll} on v_w as,

$$f_{peak}^{coll} = 1.32 \times 10^{-5}\left(\frac{0.62}{1.8 - 0.1v_w + v_w^2}\right)\Big(\frac{g_*}{100}\Big)^{1/6}\left(\frac{T}{100\,GeV}\right)\left(\frac{\beta}{H}\right)\text{Hz}, \tag{37}$$

which is interestingly similar to Eq.36. We may also observe that the peak frequency of GW due to bubble collisions does not depend very sensitively on the bubble wall velocity.

The fractional gravitational energy density (or intensity) in the early Universe is defined as,

$$\Omega_{GW} = \frac{\rho_{GW}}{\rho_{tot}} \tag{38}$$

and its relation with the corresponding value $\Omega^{coll}_{GW^0}$ at the present Universe is given by,

$$\Omega^{coll}_{GW^0} = \Omega^{coll}_{GW}\left(\frac{a}{a_0}\right)^4\left(\frac{H}{H_0}\right)^2 \tag{39}$$

Using the value of the Hubble constant in the present Universe [42], $H_0 = 2.1332h \times 10^{-42}GeV(h \simeq 0.7)$, $H^2 = (8\pi^3/90)\,Gg_*T^4 = 1.85 \times 10^{-38}g_*T^4\,GeV^{-2}$ and Eq.30, we get,

$$h^2\Omega^{coll}_{GW^0} = 0.684 \times 10^{-5} \times \left(\frac{100}{g_*}\right)^{1/3}\Omega^{coll}_{GW}. \tag{40}$$

Eq.40 gives a relation between the intensities of the gravitational waves in the early Universe and the present Universe.

The GW energy density in the early Universe is given by [51],

$$\Omega^{coll}_{GW} = k^2\left(\frac{\alpha}{1+\alpha}\right)^2\left(\frac{H}{\beta}\right)^2 v_w^3, \tag{41}$$

where, the efficiency factor (k) is defined by the equation,

$$\rho_k = k\alpha\rho_{rad}, \tag{42}$$

$\alpha\rho_{rad}$ being the latent heat and ρ_k is the kinetic energy density.

We have here,

$$\rho_{tot} = (1+\alpha)\rho_{rad} \tag{43}$$

From Eq.40 we then get,

$$h^2\Omega^{coll}_{GW^0} = 6.84 \times 10^{-6}\left(\frac{100}{g_*}\right)^{1/3} k^2\left(\frac{\alpha}{1+\alpha}\right)^2\left(\frac{H}{\beta}\right)^2 v_w^3 \tag{44}$$

A recent fit gives [21, 28],

$$h^2\Omega^{coll}_{GW^0} \simeq 1.1 \times 10^{-6} \times \left(\frac{100}{g_*}\right)^{1/3} k^2\left(\frac{\alpha}{1+\alpha}\right)^2\left(\frac{H}{\beta}\right)^2\left(\frac{v_w^3}{0.24+v_w^2}\right) \tag{45}$$

which is close to Eq.44.

The GW produced by the stirring of the plasma or by the turbulent bulk motion of the plasma is somewhat different from that due to bubble collisions. In this case the relevant

length scale is the so-called 'stirring scale' [28], which is approximately given by $L_s \approx 2R_b$, where R_b is the bubble radius. For the largest bubble, $R_b \approx v_w \beta^{-1}$. A better approximation [28] for this radius is

$$R_b \approx 3 v_w \ln\left(\frac{\beta}{H}\right) \beta^{-1}. \tag{46}$$

As frequency, $f \sim L_s^{-1}$, we get from Eq.36,

$$f_{peak}^{turb} \simeq 6.4 \times 10^{-6} \Big(\frac{g_*}{100}\Big)^{1/6} \left(\frac{T}{100\, GeV}\right) \left(\frac{1}{H R_b}\right) \text{Hz} \tag{47}$$

For the case of GW produced by turbulence, the expression of the peak intensity of the wave can be cast in the form [28, 52-55],

$$h^2 \Omega_{GW}^{turb} \simeq 3.5 \times 10^{-5} \left(\frac{100}{g_*}\right)^{1/3} \left(k \frac{\alpha}{(1+\alpha)}\right)^{3/2} \left(\frac{(R_b H)}{1 + 4\frac{3.5}{(R_b H)}}\right) \tag{48}$$

We now turn to the calculations of the frequency and intensity of GW in our model. We have written the bubble nucleation rate both as functions of temperature (Eq.3) and time (Eq.35). The rates are equal at time and temperature related by Eqs.7. From Eq.35, we get,

$$\beta = \frac{\dot{\Gamma}_N}{\Gamma_N} \tag{49}$$

Then, from Eqs.7 and 3 we obtain,

$$\frac{\beta}{H} = T \frac{d}{dT} \left(\Delta F_C(T)/T\right) \tag{50}$$

where, we have neglected the time variation of the prefactor in comparison to that of the exponent as the nucleation rate is mainly driven by the exponential factor [28].

To get the derivative $T \frac{d}{dT} \left(\Delta F_C(T)/T\right)$ at various temperatures in the desired range we have made a polynomial fit of $\Delta F_C(T)/T$ up to sixteenth power of T from its values calculated at a number of temperatures and tabulated in Table 2. The fitted polynomial is,

$$\begin{aligned} \Delta F_C(T)/T = 63631.9 - 2.88719 \times 10^6 T + 6.01409 \times 10^7 T^2 - 7.54798 \times 10^8 T^3 \\ +6.39515 \times 10^9 T^4 - 3.88944 \times 10^{10} T^5 + 1.7616 \times 10^{11} T^6 - 6.07722 \times 10^{11} T^7 \\ +1.61766 \times 10^{12} T^8 - 3.34018 \times 10^{12} T^9 + 5.34127 \times 10^{12} T^{10} - 6.55427 \times 10^{12} T^{11} \\ +6.05712 \times 10^{12} T^{12} - 4.07896 \times 10^{12} T^{13} + 1.88892 \times 10^{12} T^{14} - 5.37703 \times 10^{11} T^{15} \\ +7.09076 \times 10^{10} T^{16}. \end{aligned} \tag{51}$$

TABLE II. Values of various quantities, which are useful for studying bubble dynamics.

$T(TeV)$	$\sigma(TeV^3)$	$R_C(TeV^{-1})$	$\Delta F_C(TeV)$	$\Delta F_C/T$
0.10	0.06198	17.48	79.28	792.87
0.15	0.06197	17.46	79.15	527.68
0.20	0.06196	17.41	78.70	393.50
0.25	0.06187	17.44	78.90	315.62
0.30	0.06170	17.66	80.63	268.77
0.35	0.06153	17.89	82.54	235.85
0.40	0.06130	18.19	85.02	212.56
0.45	0.06102	18.60	88.48	196.63
0.50	0.06067	19.19	93.59	187.19
0.55	0.06023	20.00	100.91	183.48
0.60	0.05964	21.12	111.53	185.88
0.65	0.05883	22.84	128.63	197.89
0.70	0.05779	25.41	156.32	223.31
0.75	0.05634	29.53	205.89	274.52
0.80	0.05435	37.14	314.21	392.76
0.85	0.05145	56.13	679.04	798.87
0.90	0.04667	172.06	5786.28	6429.20

Differentiating the function (Eq.51) with respect to T we can get the value of β/H at a particular temperature.

In Ref.20 an expression of efficiency factor for supersonic deflagration has been derived in model-independent way:

$$k = k_1 + (v_W - c_S) \times \delta + \left(\frac{v_W - c_S}{c_J - c_S}\right)^3 (k_2 - k_1 - (c_J - c_S) \times \delta), \tag{52}$$

$$k_1 = \frac{\alpha^{2/5}}{0.017 + (0.997 + \alpha)^{2/5}},\ k_2 = \frac{\sqrt{\alpha}}{0.135 + \sqrt{0.98 + \alpha}},\ \delta = -0.9 \ln\left(\frac{\sqrt{\alpha}}{1 + \sqrt{\alpha}}\right) \tag{53}$$

and c_S and c_J are the sound and Jouguet velocities respectively.

$$c_J = \frac{\sqrt{1/3} + \sqrt{\alpha^2 + 2\alpha/3}}{1 + \alpha} \tag{54}$$

In Fig.7, we show the variation of GW signal generated by bubble wall collisions against temperature as well as the bubble wall velocity. The plot shows that the intensity is practically independent of the bubble wall velocity. This behavior can be understood from the v_w dependence of the intensity, as demonstrated by Eq.45. This feature of velocity independence has been found here in the case of frequency also as we have already mentioned. Next,

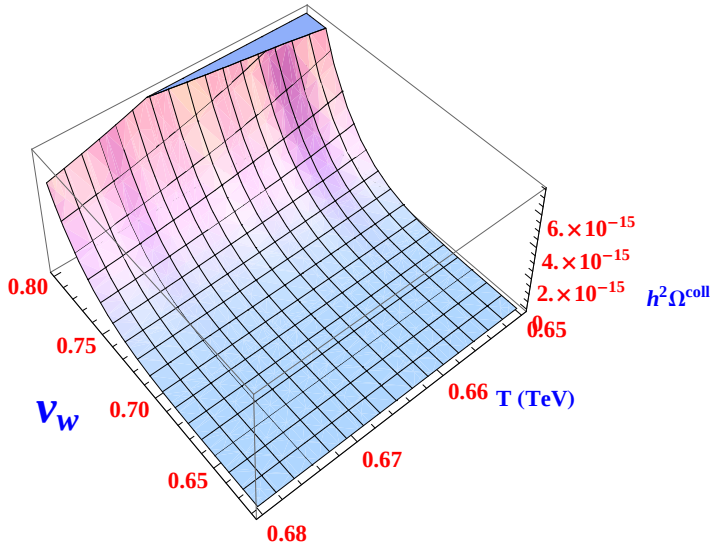


FIG. 7. Plot of variation of intensity of GW from bubble wall collisions against wall velocity v_w and temperature T.

we have compared the GW intensities for the cases of bubble collisions and turbulence for a fixed value of the wall velocity (v_w=0.7) and for temperatures above the nucleation temperature T_N=0.635 TeV, upto temperature near T_C=0.91 TeV in Fig.8. In the same figure we have plotted the value of $(\beta/H)^{-2}$. The trend of the GW signal from bubble collisions and turbulence follows the variation of the quantity $(\beta/H)^{-2}$. As the temperature is lowered from T_C, more and more bubbles are formed which eventually increases the likelihood of more bubble collisions. Thus the intensity of GW increases as the temperature approches T_N. Similarly, as the radii of the bubbles increase with decrease in temperature [see Eq.46] the stirring scale L_s of turbulence increases making the motion of the plasma more turbulent and thus the intensity of GW due to turbulence is enhanced. We also note that the signal from turbulence to be more enhanced than that from bubble collisions. Specifically, the value of the peak intensity arising out of turbulence is about 10^{-13} whereas that due to bubble collisions is 10^{-16} at temperure around T_N. The calculation shows that the turbulent

motion of the plasma was more instrumental in producing GW in the early Universe than the bubble collisions.

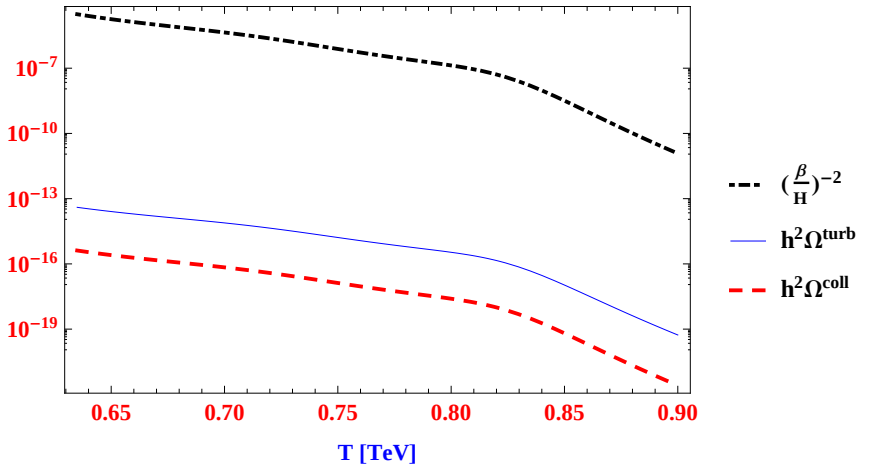


FIG. 8. Plot of Intensity of GW due to turbulence (solid line) and from wall collisions (dashed line). Bubble wall velocity is held fixed at an intermediate value, $v_W = 0.7$. Upper plot shows the variation of $(\beta/H)^{-2}$ with temperature T.

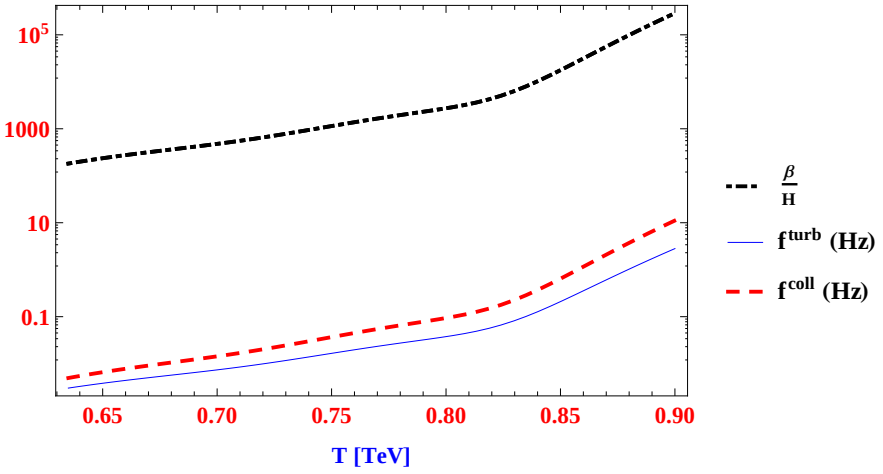


FIG. 9. Plot of frequency of GW due to bubble collisions (dashed line) and from turbulence (solid line). Bubble wall velocity is held fixed at an intermediate value, $v_W = 0.7$. Upper plot (dash-dotted line) shows the variation of $\frac{\beta}{H}$ with temperature T.

In Fig.9 we have shown the frequency distribution against temperature for GW from turbulence as well as bubble collisions. We have also plotted the variation of $\frac{\beta}{H}$ with temperature. The figure shows that the peak freuencies of GW are essentially proportional to

the values of $\frac{\beta}{H}$. The peak frequencies around the region of peak intensities are only fractions of a Hertz. The very low value of GW intensity obtained in our analysis can be understood by noting that the intensity is roughly given by (see Eqs. 45 and 48),

$$\Omega_{GW} \approx 10^{-5} k^2 \alpha^2 \left(\frac{\beta}{H}\right)^{-2} \tag{55}$$

In our model, we have got small value of $\alpha\,(\sim 10^{-3})$ and large value of $\beta/H\,(\sim 10^3)$ (obtained from Eqs.50 and 51). The low value of α is because of two reasons (see Eq. 21): (i) large number of relativistic species (=214, more than double of the SM value) present in the plasma and (ii) high temperature of the plasma (T $\sim$ TeV).

On the other hand, the GW frequency is roughly given by (see Eqs. 37 and 47)

$$f_{GW} \approx 10^{-5} \left(\frac{\beta}{H}\right) \text{ Hz} \tag{56}$$

which explains the value of peak frequency in the deciHz range.

The weak GW signals that are obtained in our calculations are difficult to detect in the ongoing GW detectors including LIGO. However, there are good possibilities of detection in Ultimate DECIGO [28] and BBO Correlated [48], as the sensitivities of these detectors conform to the frequency and intensity range obtained in the present calculation. These distinct signals of the gravitational waves are characteristic signatures of the high temperture non-standard electroweak phase transition explored [36] in LHT.

VI. CONCLUSIONS

In conclusion, we have studied in the present paper some aspects of the dynamics of the bubbles associated with first-order electroweak phase transition within the framework of the littlest Higgs model with T parity. We had earlier, in this model noticed a new region of strong first-order phase transition and proposed a baryogenesis scenario at the TeV scale. Our general observation in the present work is that the bubble wall motions are supersonic deflagrated. It may be noted that the supersonic expansion of symmetric phase bubbles has been considered recently [14] in a different baryogenesis model. We have also considered the generation of gravitational waves due to bubble collisions as well as turbulence in the plasma. As expected, the calculated intensities for the latter case are three order of magnitude larger than for the former case, at their peak values. Although the obtained intensities are quite

small in magnitude, we expect them to be detected by some of the future gravitational wave detectors.

ACKNOWLEDGMENTS

One of the authors (S.A.) acknowledges the Council of Scientific and Industrial Research, the Government of India for granting a Senior Research Fellowship, under which part of the work was done. He also thanks Ariel Mégevand for illuminating correspondences and José M. No for valuable comments. B.G. thanks Patrick Dasgupta of Delhi University for useful discussions.

---

[1] N. Turok, Phys. Rev. Lett. **68**, 1803 (1992).

[2] M. Kamionkowski and K. Freese, Phys. Rev. Lett. **69**, 2743 (1992).

[3] G. W. Anderson and L. J. Hall, Phys. Rev. D **45**, 2685 (1992).

[4] M. E. Carrington and J. I. Kapusta, Phys. Rev. D **47**, 5304 (1993).

[5] Y. Brihaye and J. Kunz, Phys. Rev D **48**, 3884 (1993).

[6] M. Laine, Phys. Rev. D **49**, 3847 (1994).

[7] J. Ignatius, K. Kajantie, H. Kurki-Suonio and M. Laine, Phys. Rev. D **49**, 3854 (1994).

[8] A. F. Heckler, Phys. Rev. D **51**, 405 (1995).

[9] J. Kripfganz, A. Laser and M. G. Schmidt, Nucl. Phys. B **433**, 467 (1995).

[10] A.E. Nelson, D.B. Kaplan and A.G. Cohen, Ann. Rev. Nucl. Part. Sci. **43**, 27 (1996).

[11] G. D. Moore, JHEP **03**, 006(2000).

[12] D. Bödekar and G. D. Moore, JCAP **05**, 009 (2009).

[13] A. Mégevand and A. D. Sanchez, Nucl. Phys. B **825**, 151(2010).

[14] C. Caprini and J. M. No, JCAP **01**, 031 (2012).

[15] S. J. Huber and M. Sopena, arXiv:1302.1044 [hep-ph].

[16] S. B. Duari and U. A. Yajnik, Mod. Phys. Lett. A **11**, 2481 (1996).

[17] P. John and M. G. Schmidt, Nucl. Phys. B **598**, 291 (2001).

[18] K. Funakubo and E. Senaha, Phys. Rev D **79**, 115024 (2009).

[19] H. Kurki-Suonio and M. Laine, Phys. Rev D **51**, 5431 (1995).

[20] J. R. Espinosa, T. Constandin, J. M. No and G. Servant, JCAP **06**, 028 (2010).

[21] S. J. Huber and T. Constandin, JCAP **05**, 017 (2008); **09**, 022 (2008).

[22] C. Caprini, R. Durrer and G. Servant, Phys. Rev. D **77**, 124015 (2008); JCAP **12**, 024 (2009).

[23] A. Mégevand, Phys. Rev D **78**, 084003 (2008).

[24] T. Kahniashvili, A. A. Kosowsky, G. Gogoberidze and Y. Maravin, Phys. Rev. D **78**, 043003 (2008).

[25] T. Kahniashvili, L. Kisslinger and T. Stevens, Phys. Rev. D **81**, 023004 (2010).

[26] J.M. No, Phys. Rev. D **84**, 124025 (2011).

[27] H. L. Child, J. T. Giblin Jr., JCAP **10**, 001(2012).

[28] L. Leitao, A. Mégevand and A. D. Sanchez, JCAP **10**, 024 (2012).

[29] M. Shaposhnikov, J. Phys.: Conference Series, **171**, 012005(2009) and references therein.

[30] N. Arkani-Hamed, A. G. Cohen, E. Katz and A. E. Nelson, JHEP **07**, 034 (2002).

[31] H. C. Cheng and I. Low, JHEP **09**, 051 (2003).

[32] H. C. Cheng and I. Low, JHEP **08**, 061 (2004).

[33] I. Low, JHEP **10**, 067 (2004).

[34] J. R. Espinosa, M. Losada and A. Riotto, Phys. Rev. D **72**, 043520 (2005).

[35] F. Bazzocchi, M. Fabbrichesi and M. Piai, Phys. Rev. D **72**, 095019 (2005).

[36] S. Aziz, B. Ghosh and G. Dey, Phys. Rev D **79**, 075001 (2009).

[37] S. Aziz and B. Ghosh, Mod. Phys. Lett. A **27**, 1250190 (2012).

[38] A. J. Buras and J. Girrbach, Acta Phys. Pol. B **43**, 1427 (2012).

[39] M. Blanke, A. J. Buras, B. Duling, S. Recksiegel and C. Tarantino, Acta Phys. Pol. B **41**, 657 (2010).

[40] The ATLAS Collaboration, Phys. Lett. B **716**, 1 (2012).

[41] The CMS Collaboration, Phys. Lett. B **716**, 30 (2012).

[42] E. W. Kolb and M. S. Turner, The Early Universe, Frontiers in Physics (Westview Press, 1994).

[43] I. Affleck, Phys. Rev. Lett. **46**, 388 (1981); A.Linde, Nucl. Phys. B **216**, 421(1983).

[44] L. D. Landau and E.M. Lifshitz, Fluid Mechanics, Pergamon Press, New York (1989).

[45] A. Mégevand and A. D. Sanchez, Nucl. Phys. B **820**, 47 (2009).

[46] P. J. Steinhardt, Phys. Rev D **25**, 2074(1982).

[47] A. Mégevand, astro-ph.CO/1303.4233.

[48] C. Grojean and G. Servant, Phys. Rev D **75**, 043507 (2007).

[49] S. Wienberg, Gravitation and Cosmology, Wiley, New York (1982).

[50] M. Maggiore, Gravitational Waves: Volume 1: Theory and Experiments, Oxford University Press, USA (2007).

[51] M. Kamionkowski, A. Kosowsky and M. S. Turner, Phys. Rev D **49**, 2837(1994).

[52] C. Caprini, R. Durrer, T. Konstandin and G. Servant, Phys. Rev. D **79**, 083519 (2009).

[53] A. Kosowsky, A. Mack and T. Kahniashvili, Phys. Rev. D **66**, 024030 (2002) ; A. D. Dolgov, D. Grasso and A. Nicolis, Phys. Rev. D **66**, 103505 (2002); G. Gogoberidze, T. Kahniashvili and A.Kosowsky, Phys. Rev. D **76**, 083002 (2007).

[54] C. Caprini and R. Durrer, Phys. Rev. D **74**, 063521 (2006).

[55] C. Caprini, R. Durrer and G. Servant, JCAP, **0912**, 024 (2009).